



Extensive air showers and atmospheric electric fields. Synergy of space and atmospheric particle accelerators

A. Chilingarian

A I Alikhanyan National Laboratory (Yerevan Physics Institute), Alikhanyan Brothers 2, Yerevan 0036, Armenia

Received 21 October 2023; received in revised form 5 March 2024; accepted 8 March 2024

Abstract

Various particle accelerators operate in the space plasmas, filling the Galaxy with high-energy particles (primary cosmic rays). Reaching the Earth's atmosphere, these particles originate extensive air showers (EASs) consisting of millions of elementary particles (secondary cosmic rays), covering several km^2 on the ground. During thunderstorms, strong electric fields modulate the energy spectra of EAS secondary particles, changing the shower size (number of EAS electrons) and altering the primary particle's estimated energy and frequency of the surface array triggers. Impulse amplifications of particle fluxes (the so-called thunderstorm ground enhancements, TGEs) manifest themselves as large peaks in the time series of count rates of particle detectors located on the Earth's surface. Free electrons are abundant at any altitude in the atmosphere, from small to large EASs. These electrons serve as seeds for electron accelerators, which operate in the thunderous atmosphere and send particle avalanches in the direction of Earth's surface and into space (terrestrial gamma flashes, TGFs). EAS cores randomly hitting arrays of particle detectors also generate short bursts of relativistic particles. For years, particle detectors, electric field sensors, and lightning locators have gathered information about the complex interactions of secondary particle fluxes, electric fields, and lightning flashes. This information is crucial for establishing a field of high-energy physics in the atmosphere.

Plain language summary: Correlated measurements of particle fluxes modulated by strong atmospheric electric fields, registration of broadband radio and optical emission from atmospheric discharges, and registration of electric fields and various meteorological parameters lead to a better understanding of the complex processes of particle-field interactions in the terrestrial atmosphere. The cooperation of cosmic rays and atmospheric physics has led to the development of models of the origin of particle bursts recorded on the Earth's surface, vertical and horizontal profiles of electric fields, initiation of lightning flashes, etc. Interdisciplinary atmospheric science primarily requires monitoring particle fluxes around the clock by synchronized networks of identical sensors that record and store multidimensional data in databases with open, fast, and reliable access. The advances in multidimensional measurements over the past decade significantly intensified the development of new integrated models of atmospheric electricity and electron acceleration, giving more insight into understanding the modulation effects posed on EAS particles in the strong atmospheric electric fields.

© 2024 COSPAR. Published by Elsevier B.V. All rights reserved.

Keywords: RREA; TGE; TGF; Particle bursts; Atmospheric electric fields

1. Introduction

Millions and millions of particles are sent toward the Earth by the most powerful natural particle accelerators operating in the Universe and in the electrified atmosphere.

Protons and fully-stripped nuclei, which are accelerated in violent explosions in our galaxy and beyond, enter the Earth's atmosphere and unleash Extensive Air Showers (EASs, Auger et al., 1939). Particle detectors arranged in large surface arrays continuously detect particle bursts, which are analyzed to determine the sources of primary particles. Modern large EAS experiments are located in

E-mail address: chili@aragats.am

<https://doi.org/10.1016/j.asr.2024.03.013>

0273-1177/© 2024 COSPAR. Published by Elsevier B.V. All rights reserved.

high-altitude regions with frequent thunderstorms, which induce strong electric fields aloft the detector. Atmospheric electric fields significantly impact the energy spectra of shower particles. They affect the shower in several ways, including the acceleration and deceleration of electrons, positrons, and muons, enhancing gamma-ray and neutron fluxes, and influencing the shower's particle density. Furthermore, strong atmospheric electric fields can lead to the emergence of relativistic runaway electron avalanches (RREAs, Gurevich et al., 1992; Babich et al., 2001; Alexeenko et al., 2002; Dwyer, 2007), causing a sizeable impulsive enhancement of the number of electrons and gamma rays in the EAS.

Understanding the relationship between cosmic rays and atmospheric electric fields is crucial for accurately identifying the type and energy of primary particles. Consequently, scientists conduct intensive simulations to study any biases introduced by atmospheric fields in the physical inferences obtained from EAS experiments. Studying cosmic ray interactions in the Earth's atmosphere also yields valuable insights into charge separation mechanisms in thunderclouds and on lightning origination. Comprehensive research with integrated particle and atmospheric physics instrumentation can reveal the reasons behind a significant increase in EAS trigger frequency during thunderstorms. This approach can also help to understand the complex atmospheric processes that cause these modulation effects and generate large particle bursts. This review investigates the relationship between EASs, lightning flashes, and the intriguing processes of high-energy physics in the atmosphere (HEPA, Dwyer et al., 2012). We intend to shed light on the complex interplay of particle fluxes, electric fields, and lightning flashes in an attempt to integrate all HEPA phenomena into one framework.

2. Electric structure of the thundercloud and particle acceleration

Thunderstorms create strong electric fields in huge areas within and around the storm system (shown by red arrows on the left side of Fig. 1). The charge separation within the thunderclouds, caused by the updraft of warm air and interactions between different hydrometeors, initiates oppositely directed dipoles within the thundercloud. In 1945–1949, Joachim Kuettner conducted groundbreaking experiments at Zugspitze (Kuettner, 1950), where he discovered the tripole charge structure of the thundercloud's charged layers. The tripole model suggests that the atmospheric electric field comprises upper and lower dipoles of different charges, accelerating free electrons toward the open space and to the Earth's surface (Fig. 1). The upper dipole comprises the main negative and main positive layers. Electrons accelerating into open space create avalanches in the upper atmosphere, resulting in copious emissions of bremsstrahlung gamma rays. The gamma glow initiated in the upper atmosphere is registered by airborne experiments flying into and above thunderstorms

(Kelley et al., 2015; Ostgaard et al., 2019). The most energetic gamma rays occasionally reach orbiting gamma observatories, creating microsecond-long bursts of particles known as terrestrial gamma flashes (TGFs, Fishman et al., 1994; Mailyan et al., 2016). The lower dipole comprises the same main negative layer and its mirror in the Earth. The third dipole emerges between the main negative layer and the transient “pocket” of the lower positively charged layer (LPCR) sitting on the falling graupel (snow pellets coated with a layer of ice, Kuettner, 1950). The electrons accelerated in the lower dipole create electron-gamma ray avalanches registered on the ground as thunderstorm ground enhancements (TGEs, Chilingarian et al., 2010; 2011). TGEs consist of millions of gamma rays, electrons, and rarely neutrons. Also, the fourth dipole between LPCR and its mirror in the Earth accelerated positrons and positive muons and decelerated electrons and negative muons. The fifth dipole between the main positive layer and its screening layer above accelerates electrons downward.

The primary mechanism for the acceleration of seed electrons to the high energies observed in TGFs and TGEs is widely considered to be the RREA, while the other alternative models focus on how the initial free electrons might be provided or how the conditions for RREA to occur are met. RREA started when electric field strength exceeded a critical value specific to the air density (Roussel-Dupré et al., 1998; Dwyer, 2003; Babich et al., 2004). Balloon experiments conducted in New Mexico (Marshall et al., 1995; Stolzenburg et al., 2007) and TGEs detected on Aragats (Chilingarian et al., 2019a, 2022a), Zugspitze (Chilingarian et al., 2024a), and Lomnický štít mountains (Chum et al., 2020) demonstrate the coherence of emerging particle fluxes and atmospheric electric fields. Measurements of the electron energy spectra during thunderstorms on Aragats Mountain confirm the RREA developed in strong electric fields above particle detectors (Chilingarian et al., 2023a). Numerous simulations have also demonstrated the exponential increase in particle numbers after the modeled electric field surpasses the critical value through distances of 1–2 km.

The left part of the diagram in Fig. 1 shows an RREA initiated by a single seed electron entering a strong electric field. However, plenty of free electrons exist from small and large EASs at each altitude. These electrons initiate numerous RREAs, and TGEs and TGFs integrate the flux of millions of RREAs. Lightning flashes reduce the negative charge above the Earth's surface, decreasing the electric field in the lower dipole below the RREA initiation threshold. This decrease leads to a weakening of RREA, eliminating high-energy particles. Nonetheless, even after the near-surface electric field strength returns to fair-weather value, the TGEs can continue due to the Radon circulation effect (Chilingarian et al., 2020a). This is due to the presence of non-stable Radon chain isotopes ^{214}Pb and ^{214}Bi , which are lifted into the atmosphere and enlarge natural gamma radiation (see the central part of Fig. 1). TGE is prolonged up to 2–2.5 h for energies below 3 MeV due to

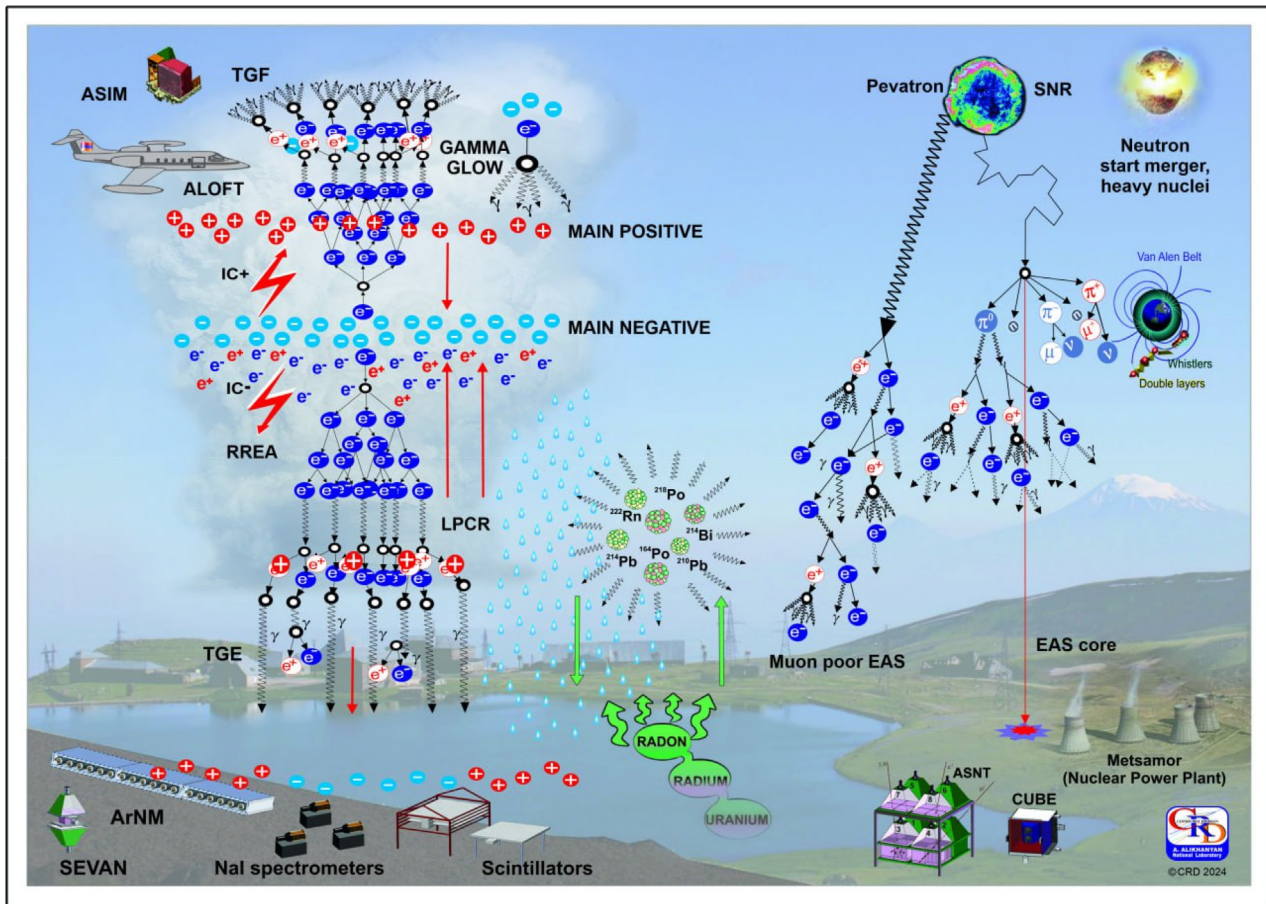


Fig. 1. The fluxes of secondary particles from space and atmospheric accelerators, as well as gamma radiation from ^{222}Rn progeny. The cartoon also shows the charge structure of a thundercloud, the direction of electric fields, lightning flashes, and various measuring facilities on the surface and in space. Additionally, we can see the sources of primary cosmic rays. In the background is the Aragats cosmic ray station, located at 3200 m and equipped with various particle detectors and spectrometers.

^{214}Pb and ^{214}Bi isotopes with half-lives of approximately 27 and 20 min, respectively.

The diagram on the right depicts the EASs born in the high atmosphere by gamma rays and protons interacting with atmosphere atoms. High-energy particles are produced during violent explosions and mergers in the Galaxy and beyond. We show in the cartoon the supernova remnant and neutron star merger. However, there are also other sources of ultra-high energy particles; this field is actively investigated by new large experiments, reviewed in the next section. EASs, upon reaching the Earth's surface, can cover several square kilometers of area. The EAS cores contain the highest energy secondary particles, which originate a very short compact bursts shown by the red circle. Muon-poor events registered at altitudes above 4000 m indicate Pevatrons, the stellar sources enable to accelerate protons up to 10^{15} eV. We also show the nuclear power plant, a possible source of radioactive contamination, and the Van Allen belt that can send MeV electrons toward the Earth's surface.

The multiple secondary particles of various types and energies are monitored 24/7 by Aragats Space Environ-

mental Center's facilities (ASEC, Chilingarian et al., 2005) and spectrometers onboard orbiting gamma observatories and aircraft. The ASEC instrumentation, shown at the bottom of the cartoon, appears in many publications and is described in detail (Chilingarian et al., 2022b; 2022c; 2022d). Here we will present the new instruments recently providing the key evidence on the particle acceleration in the upper atmosphere.

The Atmosphere-Space Interactions Monitor (ASIM, Neubert et al., 2019) on board the International Space Station (ISS) consists of two types of instruments: the X- and gamma-ray spectrometers and the multispectral imaging arrays. The high energy detector (HED) comprises 12 bismuth-germanium-oxide (BGO) bars coupled to a photomultiplier tube (PMT). The temporal resolution of the HED is determined by a dead time of ≈ 550 ns. The optical wide field facilities of ASIM comprise two imaging cameras operated at up to 12 frames per second (337 and 774 nm) and three high-speed photometers at 337 nm (bandwidth 5 nm), 180–230 nm, and 777.4 nm (bandwidth 4 nm) with a 100 kHz sampling rate. The absolute time tagging of the ASIM instruments is not worse than 20 ms, reaching a

10 μ s accuracy when using timestamps from the lightning location networks. Thus, ASIM has unprecedented possibilities to register sequences of particle fluxes and lightning flashes in the upper atmosphere.

Airborne Lightning Observatory (ALOFT, Ostgaard et al., 2023) has a comprehensive set of instruments on NASA's ER-2 research aircraft. The ER-2 flew at \approx 20 km altitude, above thunderstorms. An imaging array of photometers sensitive to different wavelengths and advanced electric field meters accompanies observations of high-energy electromagnetic radiation. The lightning instrument package gives three components of electric field measurements. Ground-based networks of lightning mapping facilities provide additional data during the flights.

3. Change in the frequency of EAS triggers during thunderstorms

In the previous section, we mentioned five dipoles that modulate particle fluxes entering electric fields in thunderclouds. Correspondingly, we listed several sources of impulsive fluxes: RREAs, EASs, and Radon progeny. Entering this complicated electrical environment, electrons from the EASs will be accelerated and multiplied in the atmospheric electric field. This will cause significant changes in the secondary electron energy spectrum, which will affect the density and energy of registered electrons, leading to biases in the primary particle energy estimates (Chilingarian, 2023). The array trigger rate will also be enhanced.

Early measurements of the EAS-TOP detector in Italy (Aglietta et al., 1989) indicated a significant increase in the EAS trigger rate during thunderstorms. In recent times, modern high-altitude experiments have paid great attention to possible biases caused by the propagation of EASs through strong atmospheric electric fields.

The ARGO-YBJ experiment (Axikegu et al., 2022) is an ideal platform for researching the modulation effects of electric fields on EAS because of its high-altitude location on the Tibet plateau (4300 m), where thunderstorms occur frequently. Moreover, the central full-coverage carpet makes it possible to measure particle density accurately. The experiment had two independent data acquisition systems: scaler and shower operation modes. In scaler mode, the counting rate of each detector cluster was measured every half a second. In shower mode, the detector was triggered when at least 20 pads in the central carpet were fired within 420 ns. They found a 20 % increase in the EAS triggers in 2012. The mean duration of 20 episodes of enhanced trigger rates is well linked with thunderstorms. The Monte Carlo simulation, performed for various strengths and polarities of the field (\approx 0.2 kV/cm), accurately corresponds to the observations concerning the amplitude and sign of the trigger rate variations. The simulations assumed a uniform electric field of 500 m above the detector. Trigger rate variations depend on the near-surface electric field (NSEF) sign, measured by BOLTEK's

electric mill EFM 100 (BOLTEK, 2024). If NSEF is positive, the count rate decreases; if negative, it increases. The trigger rate gradually changed with varying NSEF during the 1.5 h of the storm. They also noted that the NSEF has more effects on EAS triggers at larger zenith angles.

The LHAASO surface array (Aharonian et al., 2023), located at Haizi Mountain in Daocheng County, Sichuan Province, is situated at the edge of the Tibetan Plateau, with an altitude of up to 4410 m. The Tibetan plateau is known for frequent thunderstorms and large intracloud electric fields, whose vertical profile can extend to 1–2 km. The largest component of LHAASO, KM2A, comprises 5216 electromagnetic particle detectors (EDs) and 1188 muon detectors (MDs). The ED array covers an area of 1.3 km² in a triangular grid. The EDs detect the electromagnetic particles in the shower, which are used to reconstruct the shower core position, arrival direction, and primary particle energy. EAS trigger logic requires at least 20 EDs fired within a time window of 400 ns. The DAQ records 10 μ s of data from all EDs and MDs for each shower event with signals over the thresholds. Between October 2019 and March 2022, the BOLTEK field mill EFM 100 detected more than 200 thunderstorm events at the LHAASO observatory. Most of them were recorded between April and September. During this time, a significant increase was observed in the number of particles (EAS size Ne) detected by the ED array (approximately 20 %) and in the trigger rates (approximately 20 %).

The High Altitude Water Cherenkov (HAWC, Abeyssekara et al., 2012) observatory is in the saddle region between the Sierra Negra and Pico de Orizaba in Mexico. It sits at an elevation of 4100 m above sea level. Due to its high altitude, the observatory is affected by electrically charged clouds and lightning flashes for around six months of the year. HAWC comprises 300 water Cherenkov detectors (WCD), each overviewed by 4 photomultiplier tubes (PMTs). They are spread across an area of 20,000 m², and each WCD measures 7.3 m in diameter and 5.0 m in depth. The main data acquisition (DAQ) system records the arrival times and time over thresholds of PMT pulses. It also includes a time-to-digital converter (TDC) system that counts the hits within a 30 ns time window of each PMT and the coincidences of 2, 3, and 4 in each WCD. Recently, a small and fast scintillator (7.62 \times 7.62 cm LaBr3) was placed near the giant water-Cherenkov detectors of HAWC (Bowers et al., 2021). The detector output was attached to the Broadband Interferometric Mapping and Polarization (BIMAP) sensor's electronics. BIMAP captures 15 ms of data for each trigger, with 5 ms of pre-trigger data. This detector observed particle bursts between September 2017 and September 2019 on fair-weather days, meaning there were no nearby lightning flashes (see Tab. 1 of Bowers et al., 2021). CORSIKA (Heck et al., 1998) simulations confirm that particle bursts originated from EAS core particles captured in nuclei of soil, which produced high-energy gamma rays through (n, γ) reactions. HAWC's

particle bursts are initiated by EAS core particles hitting the HAWC array and are unrelated to atmospheric discharges.

Lara et al. (2017) conducted a study where they observed that the HAWC scaler system detected an increase in the count rate during thunderstorms with a strong negative electric field. The study found no significant changes in atmospheric pressure during the count rate enhancement. It's worth noting that no significant enhancements were observed during positive fields.

The Pierre Auger Observatory (AUGER, 2004) is a large ground-based experiment in the Argentinian Pampa. Covering an area of 3000 km², it is used to identify ultra-high energy cosmic rays. The experiment consists of two parts - the surface detector and the fluorescence detector. The surface part has 1660 water-Cherenkov detectors, which sample the footprint of the air showers as they hit the ground. The fluorescence detector has 27 telescopes that record the longitudinal development of EAS in the atmosphere by registering the fluorescence light. During thunderstorms, the surface detector observed peculiar lightning-related events that differed from an extensive air shower. These events cover an area of about 200 km², much larger than the footprint of EAS events, and their signals last more than 20 microseconds, an order of magnitude longer than EAS signals (Colalillo et al., 2023). Unfortunately, the detection rate for these events is low, as there is often a lack of signal in the center of the footprint. It has been verified that this is not due to physical reasons but to the Auger trigger being optimized for EAS events.

The Telescope Array (TA, Abbasi et al., 2018) experiment includes a large surface detector called the TASD, with 507 scintillator detectors placed in a 1.2-km square grid over 700 km². The TASD can provide information about the shower footprint, such as core location, lateral density profile, and timing, which can be used to determine the shower axes and energy. Each measuring unit has upper and lower scintillators, which are 1 cm thick and cover a 3 m² area, separated by a 1-mm-thick steel plate. The scintillators are read out by photomultiplier tubes via an array of wavelength-shifting fibers, and a 12-bit ADC digitizes the output signals with a 50-MHz sampling rate. An event trigger is recorded when three adjacent units detect a signal larger than three vertical equivalent muons (VEMs) within eight microseconds. The trigger frequency is ≈ 0.01 Hz. The changing count rates of the TA scintillators can be used to detect deficits or excesses in the cosmic ray intensity, which correlate with thundercloud movement. These variations in intensity move in the same direction as the thundercloud for tens of minutes at a speed of approximately 2 km/min. These changes are also associated with lightning flashes and atmospheric electric fields without lightning. The observed intensity variations were caused by an electric field magnitude (potential difference) of approximately 200–400 MV (Abbasi et al., 2022).

The TASD system records trigger events in intervals of 1 ms, closely associated with lightning flashes above the

TA detector. These lightning flashes are detected by the Lightning Mapping Array (LMA) and the Vaisala National Lightning Detector Network (NLDN). There were ≈ 750 NLDN-recorded flashes (IC and -CG) per year above the 700-square-kilometer T ASD array. However, over eight years of TA operation, only 20 bursts were detected that were correlated with lightning activity. This means that less than 0.5 % of NLDN flashes recorded over the T ASD had identifiable gamma bursts accompanying them. The bursts lasted for several hundred microseconds, and the source was typically a few kilometers above ground level. In (Belts et al., 2020) the authors proposed a lightning-related scenario for the origin of the bursts: “The results show that TGFs occur during strong initial breakdown pulses (IBPs) in the first few milliseconds of -CG and low-altitude intra-cloud flashes, and that the IBPs are produced by a newly-identified streamer-based discharge process called fast negative breakdown.”

In the late 20th century, the MAKET ANI surface array on Aragats became the first instrument to measure the energy spectra of both light and heavy galactic nuclei separately (Chilingarian et al., 2004). The results showed a sharp knee in the light component at 2–3 PeV, while no knee was observed in the heavy component up to 10 PeV. After finishing high-energy astrophysics experiments, we keep sixteen 1 m² area and 5 cm thick plastic scintillators for HEPA studies. The trigger condition was the detection of signals from at least eight scintillators within one microsecond. During the TGEs on 19 September 2009 and 4 October 2010, the MAKET triggers were enhanced by 250 %, as shown in Fig. 2 of Chilingarian et al. (2011). To identify RREA events, we used the mean and maximum particle densities recovered by counts in 16 scintillators. The densities of TGE particles originating from multiple RREAs in the thundercloud above with maximum energy not exceeding 50 MeV are expected to be uniform without any significant peaks. The typical particle density distribution of the EAS hitting Earth's surface is bell-like, with a substantial fraction of the shower particles near the EAS core. Thus, if the EAS core is near scintillators, enormous densities can occur, and the mean density is expected to be larger than one from RREA. The linear discrimination function in 2-dimensional feature space suppressed approximately 50 % of the “pure” EAS events, losing approximately 25 % of the joint EAS and TGE events (148 from 613, see Figs. 3, 4 of Chilingarian et al. (2011)). The 25 % contamination could not be significantly reduced due to large EASs with axes far from the MAKET array. After analyzing 465 selected ECSe (Extensive Cloud Showers), also called microbursts by Alex Gurevich (Gurevich et al., 1999), we found that ECSe are distributed uniformly within a 100-meter radius, limited by the size of the MAKET array.

The next section will present a detailed analysis of how the atmospheric electric fields produce TGEs and TGFs.

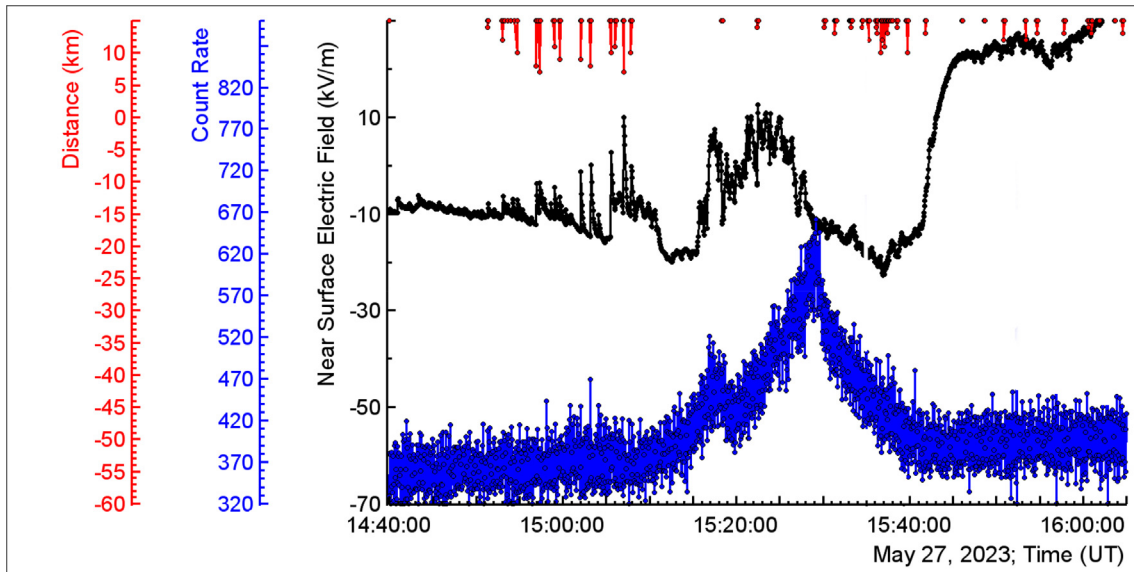


Fig. 2. 50 ms time series of 1 cm thick 1 m² area plastic scintillator, blue; disturbances of near-surface electric field measured by BOLTEK's EFM 100 electric mill, black; distances to the lightning flash, red.

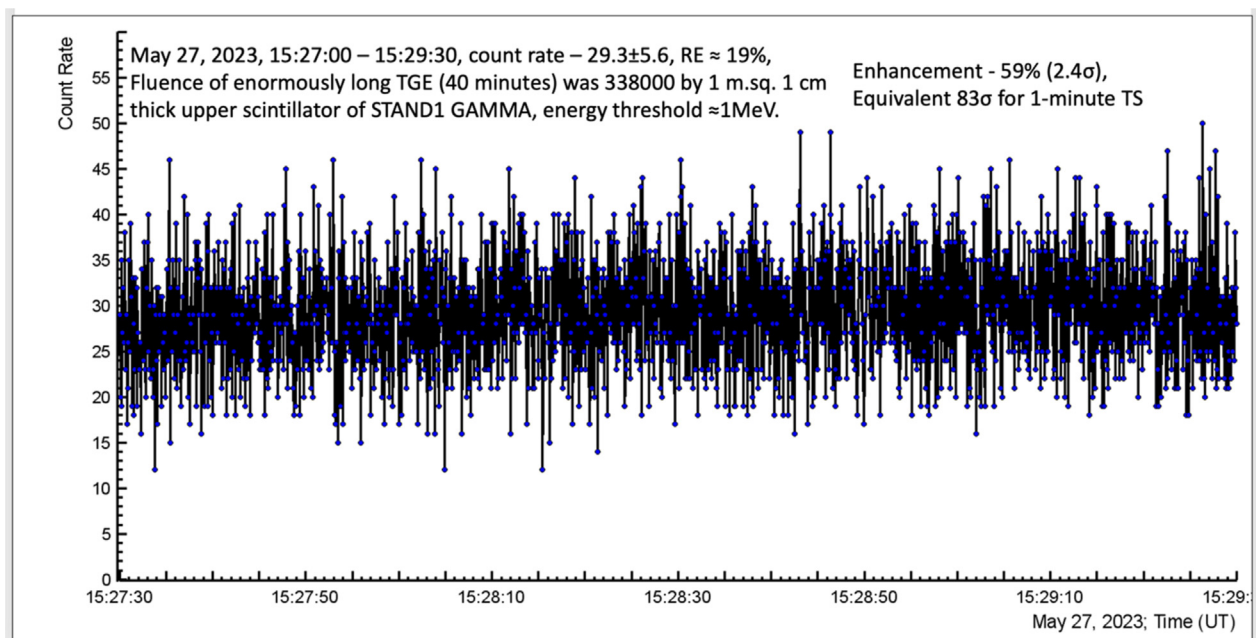


Fig. 3. The count rate of 1 m² area and 1 cm thickness scintillator (energy threshold \approx 1 MeV); two minutes of maximum TGE flux.

4. TGEs and TGFs: Origination and measurement conditions

In large-scale electric fields, free electrons accelerate and multiply, forming RREAs. RREAs can reach spaceborne detectors and be registered as TGFs, and they can reach the ground and be registered as TGEs. TGEs and TGFs are developing within large-scale strong atmospheric electric fields aligned within the lower and upper dipoles in the thundercloud. Large surface arrays in Tibet and Utah confirmed that enhancement of the particle detector count rates correlates with the movement of thunderclouds with

strong electric fields inside. The observed by Torii et al. (2011) “migrating” radiation source along the west coast of the Sea of Japan was consistent with the movement of clouds between remote ground-based detectors according to wind direction and speed. TGEs registered at Aragats by particle detector networks covering a 50,000 m² area demonstrate very stable uniform particle flux of fluence above tens particles/cm² (Chilingarian et al., 2024a). The disturbances of NSEF accompanied by TGEs were observed approximately simultaneously at the slopes of Mt. Aragats, separated by \approx 13 km. Equivalently, the

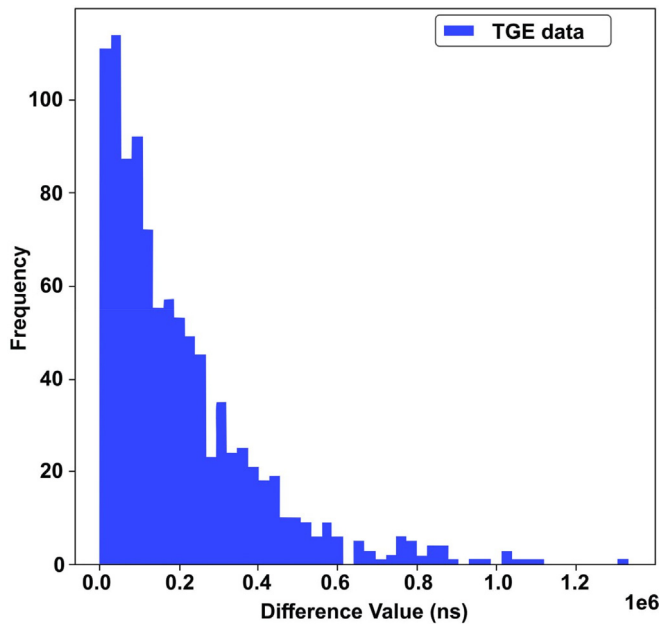


Fig. 4. Histogram of the KS test statistics for pair-wise comparison of MAKET and 100 Poisson distributed samples.

ALOFT mission onboard NASA's ER-2 aircraft, flying above the violent thunderstorms in the equatorial regions, registered hundreds of gamma-ray bursts with duration from microseconds to minutes (Ostgaard et al., 2023). Thus, if detectors are as near to the radiation sources as TGEs and ALOFT, minute-long particle fluxes over large areas are registered. In equatorial thunderstorms, as was anticipated, RREAs generate millions of particles in the upper dipole. The time duration of TGEs, measured by spectrometers located 25–200 m below the particle sources, and TGFs, previously measured by gamma observatories orbiting 400–600 km from the sources, differ due to crucial differences in the particle density of RREAs just going out of the acceleration electric field and many hundred kilometers far from it. The altitude of the detector relative to the particle source in the thundercloud crucially influences the observed characteristics of the gamma-ray bursts. When a detector is brought close to the sources by ALOFT, the difference in duration of TGEs and TGFs vanishes. TGEs and TGFs are essentially the same phenomena observed from different vantage points and at different stages of particle flux density. Thus, they are equivalent phenomena and can be considered two sides of the same coin. Future research would verify the similarities in the spectral and temporal characteristics of TGEs and TGFs when observed from comparable proximities to the source. The planned research on TGF involving aircraft and balloons flying above thunderclouds (Pallu et al., 2023) will establish a realistic TGF model, following the main lines of the well-developed TGE model.

TGEs have been extensively researched in the last decade (Chilingarian et al., 2019b; 2021a; 2021b; 2023b), with numerous papers published and catalogs and datasets high-

lighting different aspects of their physics available to the public (Soghomonyan et al., 2021a; 2021b; Chilingarian and Hovsepyan, 2021; Chilingarian et al., 2022f; 2024c). Electron and gamma-ray energy spectra have been recovered, intensities calculated, and their relation to thundercloud's charged structure and lightning flashes occurrences has been established. During the first TGE research campaign on Eastern Europe and German mountaintops (Chilingarian et al., 2021d; 2024b), with the same type of SEVAN particle detectors (Chilingarian et al., 2009), registered TGEs share many same characteristics. TGEs were observed mostly at large negative NSEF. However, there were TGEs detected at large positive NSEF as well. Peak enhancement varies from ten to thousands of percent for extreme TGEs registered on Aragats, Lomnicky Stit, and Musala mountaintops. Duration varies from seconds to tens of minutes. Lightning flashes abruptly terminated particle flux, and TGE started anew after the potential difference recovered. The energy spectrum prolonged up to 50 MeV. The largest TGEs were accompanied by sizeable neutron flux. The methodology of the TGE multivariate analysis is well-established and has been tested on hundreds of TGEs observed on Aragats during the last 15 years (Chilingarian et al., 2022a). These techniques are illustrated below, taking as an example a large TGE recently registered on Aragats.

On May 27th, 2023, an extended TGE occurred, lasting ≈ 30 min and resulting in a large fluence of approximately $34 \text{ particles/cm}^2$ with energies above 1 MeV. Fig. 2 displays a 50-millisecond time series of count rates from a plastic scintillator of 1 cm thickness and 1 m^2 area near the GAMMA experimental hall on Aragats. During the flux maximum, which lasted for ≈ 5 min, the scintillator count rate in 50 ms increased by approximately 60 %, from 18.4 to 29.3. Lightning activity was suppressed during the TGE, and TGE ended smoothly after reaching its maximum flux.

Along with particle flux measurements, we keep a constant watch on the atmospheric conditions at Aragats, and this data can be accessed for the past 15 years on the Cosmic Ray Division (CRD) database (ADEI, 2024). We monitor the detector noise meticulously throughout the operation of the detectors. The count rates' mean and variances are continuously measured and analyzed for any possible false signals. To avoid any anomalies, we validate the peaks in the time series using independent detectors.

As shown in Fig. 2, there were several near lightning flashes at distances nearer than 10 km between 3:00 PM and 3:10 PM, as well as attempts to initiate a TGE. However, lightning activity prevented the development of RREA in the cloud, leading to a continuous decrease in potential differences. The TGE flux began to rise after 3:10 PM when lightning activity decayed, and NSEF was in the negative domain. The rise continued when the NSEF touched the positive domain and reached its maximum at the return of the NSEF to the negative domain. The dependence of the TGE flux on NSEF, lightning occurrences,

and various weather parameters is not direct and is difficult for research because of the lack of direct measurements inside the thundercloud. However, as shown below, particle flux can be very stable for a few minutes. It is worth noting that the 30-minute-long TGE significantly differs from the other five largest TGEs of 2023, which lasted between 3 and 5 min.

In Fig. 3, we show the 50 ms time series of the count rate of the upper scintillator of the outdoor STAND1 network (the detector near the GAMMA experimental hall). The Figure legend shows the count rate mean value, standard error, and relative error. Also, we show the TGE peak's significance recalculated for a minute time series (a standard adopted for the TGE significances comparisons) that reaches 83σ (83 standard deviations from the mean value of the background measure before TGE). The TGE particle flux was stable for 2 min, demonstrating that at exceptional weather conditions, an electron accelerator can send rather stable particle flux in the direction of the Earth's surface.

In (Chilingarian et al., 2024a), we performed a statistical analysis of the particle arrival time series on a nanosecond time scale using the largest TGE event on record, which occurred four days earlier, on May 23, 2023. A 3 cm thick scintillator is connected to a two-channel digitizing oscilloscope (Picoscope 5244B). If the count rate of the 1-second time series exceeded the prechosen limit (usually set to 50% larger than the running mean of the count rate), the electronics produced the trigger for the oscilloscope (see for detail Fig. 2 of Chilingarian et al., (2024a)). The oscilloscope record length was 200 ms (992 particles were registered), and the sampling rate of signals was 250 MS/s, corresponding to the sampling intervals of 4 ns. The typical duration (full width on half maximum, FWHM) of individual pulses from the scintillator is 20–30 ns. Thus, usually, the signal occupied several sampling intervals. A detailed description of fast DAQ electronics based on the NI MyRIO board can be found in (Pokhsraryana, 2015). From our analysis, the flux of RREA particles arrives at the Earth's surface independently and uniformly for many seconds, overpassing the fair-weather flux more than ten times. Our findings confirm that the TGE is a mixture of multiple runaway electron avalanches that sustain stable flux for a few minutes. The information about the particle sources, which come from a single seed electron at a certain altitude, is entirely blurred due to the large spatial dispersion of millions of secondary particles. To demonstrate that the arrival time of TGE particles follows exponential interarrival time distribution (directly connected to Poisson distribution), we conducted a Kolmogorov-Smirnov (KS) test to compare a sample distribution with a reference probability distribution. Our approach involved generating a hundred independent samples, each containing 992 time-stamps (same as the TGE sample), distributed according to Poisson distribution. Then, we performed a pairwise KS test for the TGE and each of the 100 Poisson samples, and the KS test results were stored in a histogram. Fig. 4

displays the histogram of hundred pairwise comparisons of the MAKET data with samples from reference Poisson distribution.

The mean value of the KS test averaged by 100 values was 0.036, corresponding P-value of 0.544. Based on the high P-value of the KS statistics, it is evident that there is no difference between the distribution of TGE particle arrivals and test Poisson distributions. Thus, TGE particle arrivals occur independently and uniformly, and the time intervals between their arrivals follow a Poisson process.

5. Particle fluxes and lightning flashes

There is plenty of evidence, starting from the first balloon and NASA's/F⁰⁶ jet flights (Parks et al., 1981; McCarthy and Parks, 1985) to recent aircraft-based observations (Kelley et al., 2015; Kochkin et al., 2017; Ostgaard et al., 2019), that lightning suddenly stops particle fluxes in the upper atmosphere. TGEs provide vast information on particle-lightning relations in the lower atmosphere (Chilingarian et al., 2015; 2017a). TGEs can be abruptly terminated by normal polarity lightning (+IC) and cloud ground flashes (-CG). If a LPCR emerges (Kuettner, 1950), two other types of atmospheric discharges can terminate TGE (Nag and Rakov, 2009), namely the inverted ICs occurring between the mid-level negative charge region and the LPCR and hybrid flashes (an inverted IC followed by a -CG). Chilingarian et al. (2020b), introduced a new classification of atmospheric discharges that suddenly ended the enhanced flux of atmospheric electrons and gamma rays; we present the first experimental evidence that the conditions for TGEs can be created between the mid-level negative charge region and the LCPR. The research methodology was based on a multivariate analysis of intensity measured by large scintillators, near-surface electric fields, and fast E-field waveforms recorded with a circular flat-plate antenna. Our methodology also included the lightning type determination algorithm, first published by (Chilingarian et al., 2017b). The Mendeley dataset (Soghomonyan et al., 2021a, 2021b) included 165 TGEs terminated by lightning flashes on Aragats in 2013–2021. Fig. 5 presents an example of the TGE-lightning relations with five attempts to start TGEs on a stormy day with multiple nearby lightning flashes. Lightning activity is very low during episodes of enhanced particle fluxes lasting from several tens of seconds (TGE1, TGE2, TGE4) to several minutes (TGE3, TGE5). Lightning flashes that terminate TGE can lower the NSEF (TGE1, TGE2, and TGE4) and enhance it (TGE3 and TGE5). TGEs develop in periods between flashes. Other flashes to the left and right from 5 indicated ones also stop starting enhancements of particle fluxes. However, they are too small to be seen in the Figure.

Thus, lightning flashes in the lower and upper atmosphere abruptly terminate particle fluxes due to lowering the potential difference between charged layers in the cloud. However, another scenario of lightning-particle flux relation is adopted to explain “satellite-observed” TGEs (dif-

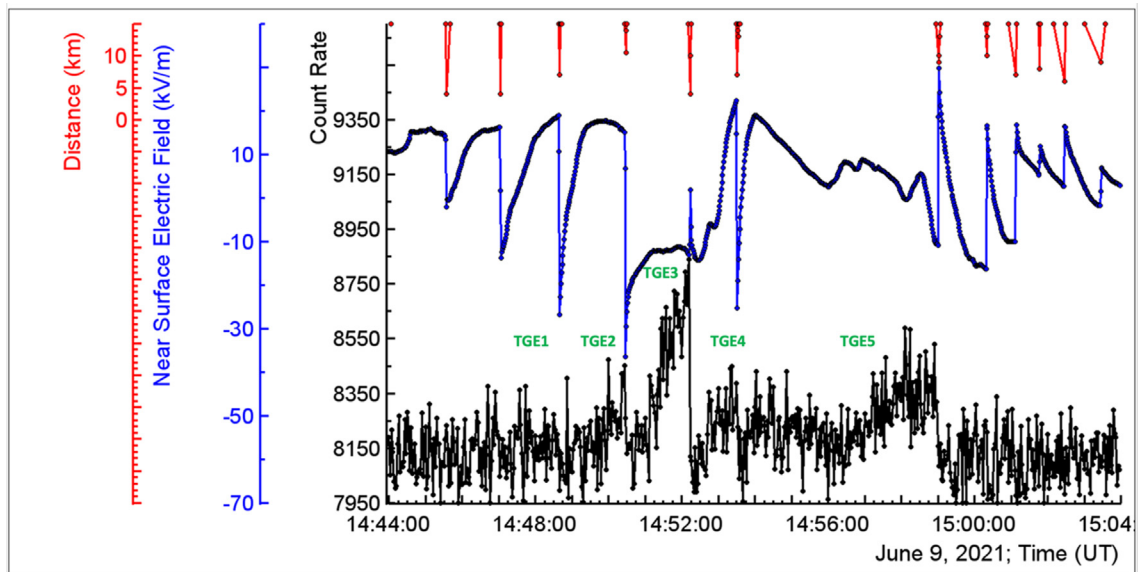


Fig. 5. 2-second time series of count rates of 4 m² area and 60 cm thickness scintillator, black; disturbances of the NSEF, blue; distances to lightning flashes, red.

fering from ALOFT-registered ones). To justify a TGF model based on “standard” vertically oriented TGF, it is suggested that a small-scale E-field at the lightning leader tip can be strong enough to start RREA and provide abundant seed electrons to create an extremely bright source with up to 10²⁰ fluence (cold runaway model, Celestin & Pasko, 2011). However, such large electric fields were never measured, and a point source of such brightness looks a bit awesome. Additionally, recent measurements and reanalysis of TGF catalogs do not support the “lightning” scenario of TGF origination. From the LOFAR measurements (Trinh et al., 2020) for cosmic-ray events accompanied by strong electric fields, no lightning activity was detected within a 100 km distance. Measurements of TGFs, taken in conjunction with the optical detection of lightning flashes by the ASIM instruments, suggest that TGFs occur 1.4 ms before the onset of optical pulses (Skeie et al., 2022). In multi-pulse patterns of TGFs registered by ASIM (see fig. 6.6 of Fuglestad, 2023), we can see that the first TGF detected at 18:02:25 on 5 July 2021 smoothly finished, and no optical images of the atmospheric discharges were observed. The second TGF, which occurred 2 ms later, was terminated by a lightning flash, as seen both in particle flux abruptly termination and by optical signal. Zhang et al. (2021) showed that gamma rays are produced several ms before a narrow bipolar event (NBE), which often marks the lightning initiation. Furthermore, analysis of four TGF catalogs from different instruments revealed that a significant proportion of TGFs lead to increased lightning activity detected in radio waves (spherics) between 150 and 750 ms after TGFs occur (Lindanger et al., 2022). This suggests that TGFs can act as precursors of lightning and initiate lightning flashes, whereas lightning activity does not produce any additional seeds for RREAs. Another scenario of “satellite” TGF origination, the feed-

back process in which positrons and gamma rays from RREA avalanche travel back up to the thundercloud and restart RREA, was never measured in the experiment and has not been confirmed in the TGE research (Chilingarian et al., 2017a). The facilities onboard aircraft flying above thunderstorms in equatorial regions already observe minutes-long TGFs comprising millions of particles (Ostgaard et al., 2023).

In Fig. 6, we compare the 10 ms duration time series of the multi-pulse TGF registered by ASIM (Fuglestad, 2023), a detector specially designed for TGF detection, and the same duration time series from the STAND1 detector, which registered a large TGE on May 23, 2023. ASIM detector is much more efficient in registering gamma-ray bursts than other orbiting gamma laboratories: RHESSI (Smith et al., 2005), Fermi (Briggs et al., 2013), and AGILE (Marisaldi et al., 2010). ASIM was designed to detect gamma rays from violent explosions in the Universe and does not use complicated off-line triggers for finding TGFs coming from the Earth’s direction.

The light pulse from ASIM’s BGO is several hundreds of ns long; therefore, it has an effective time resolution of about 1 μs. The size of the BGO detector is 900 cm². The STAND1 detector attached to a digitizing oscilloscope registers the time series of the TGE particle arrival times. It is 3 cm thick, 1 m² area upper plastic scintillator of the stacked detector array. The FWHM of the photomultiplier pulse is 30–40 ns, the sampling rate of the digitizing oscilloscope is four ns, and the detector size is 10,000 cm². Fig. 6a shows a very intense gamma-ray burst (left side) followed by a few gamma rays. In Fig. 6b distribution of particles is more-or-less uniform. The difference between “satellite” TGFs, which last for a few milliseconds, and TGEs, which last for minutes, is due to the distance between the particle source and the detector. TGEs are

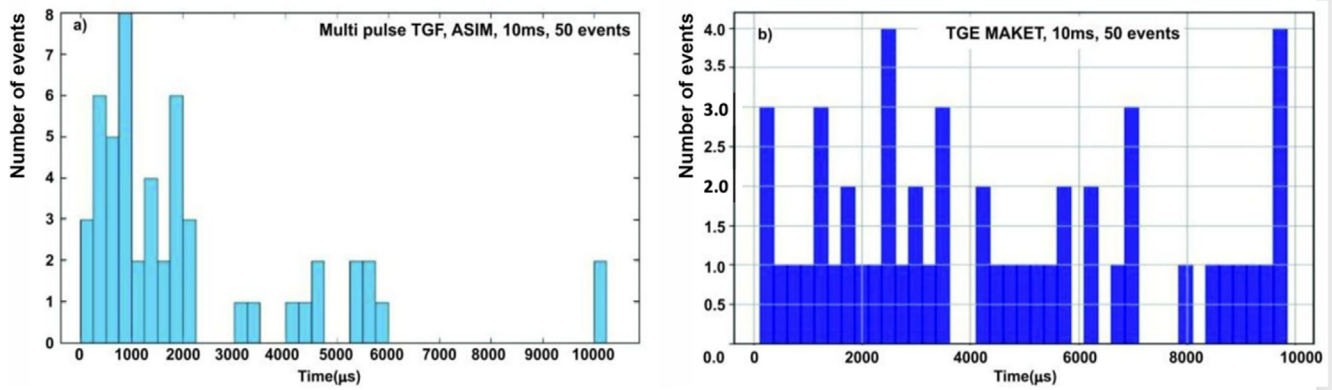


Fig. 6. a) time series of gamma-ray arrival times from the onset of the first tgf until the onset of the last tgf, registered by asim’s hed detector (adopted from (Fuglestad, 2023, Fig. 6.1); b) Time series of the TGE particle arrival times registered by STAND1 (MAKET); zero time corresponded to 00:34:53.1 on May 23, 2023. The bin width of both is 250 μ s.

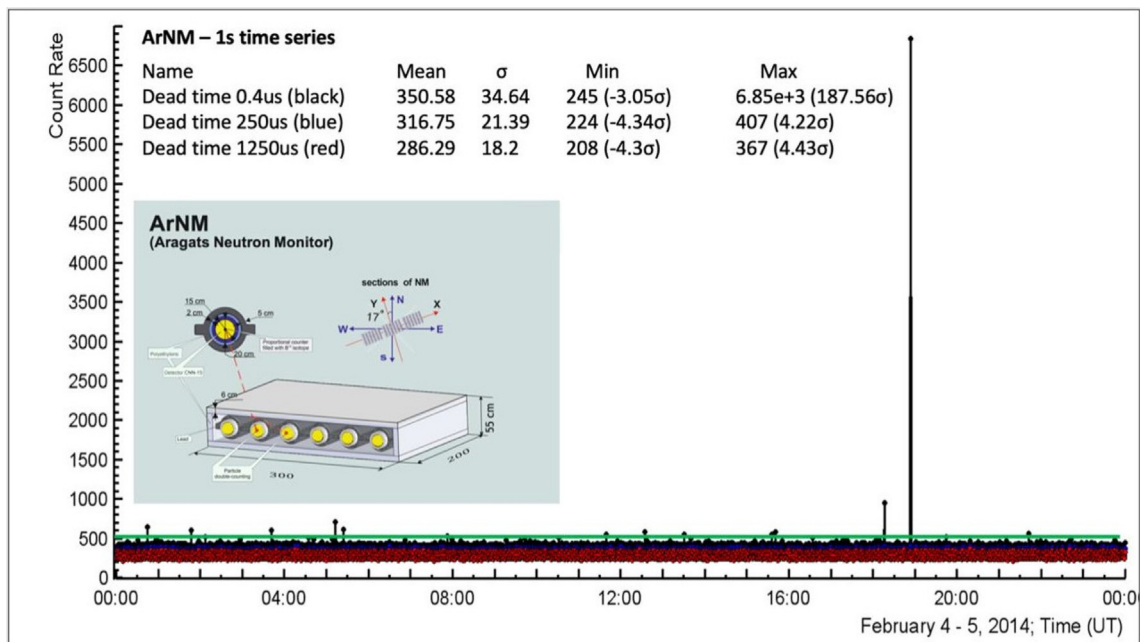


Fig. 7. 1 s time series of ArNM for three different dead times; in the inset is shown the layout of one section of the 18NM64 neutron monitor. The green line outlines 13 bursts with multiplicity above 500, corresponding to a peak significance of 5 σ relative to the mean value of the ArNM count rate.

detected \approx 1000 times closer to the particle source than TGFs. Only the most energetic gamma rays from RREAs can reach the Space Station 400 km from the Earth, producing a short particle burst, sometimes followed by a few more rounds (multi-pulse TGFs registered by ASIM, see figures in Fuglestad, 2023). On Aragats, RREAs create an almost continuous flow of particles (see Fig. 3) because of the proximity to the source detectors exposed to the particle beams from the in-cloud accelerator.

5.1. Cores of the extensive air showers (EASs) as the origin of particle bursts

The physics of particle bursts is associated with both the EAS phenomenon and the operation of electron accelerators in thunderclouds. The TA experiment relates these

bursts to lightning activity (Abbasi et al., 2018). However, recent observations put the start of TGF before the lightning flash (Ostgaard et al., 2022), and as we show in Figs. 2 and 5, minute-long TGEs develop at the depressed lightning activity. In the previous sections, we demonstrate the equivalence of TGE and TGF, which share the origination mechanism. There is also another, not well known to the community, mechanism that originates short particle bursts on the Earth’s surface. Most of the EAS’s highest energy particles are located in its core around the EAS axes. Simulations of air showers produced by high-energy protons show that their footprint covers areas of the circle of a 5–10 m radius. These particles come within a few tens of nanoseconds. A plastic scintillator from the surface array with a usual dead time of 1 μ s will generate only one large pulse (or saturated) in response to multiple parti-

cles from the EAS core and miss particle bursts. However, due to interactions of relativistic hadrons and gamma rays with soil and detector matter, it will be possible to register particle bursts with “slow” detectors. For detecting bursts of thermal neutrons, the HAWC experiment uses a small scintillator (Bowers et al., 2021). In Yangbajing (Bartoli et al., 2016), LHAASO (Li et al., 2017), and URAN (Izhbulyakova et al., 2020) experiments, thermal neutrons were measured with electron-neutron (EN) detectors (Stenkin, 2009). In the Aragats (Chilingarian and Hovsep-yan, 2022 g) and Tien Shan mountains (Chubenko et al., 2016), neutron monitors (Moraal et al., 2000) were used for burst detection. Below, we describe the burst detection with Aragats neutron monitor (ArNM).

The ArNM consists of 18 gas-filled cylindrical proportional counters of CHM-15 type (length 200 cm, diameter 15 cm) enriched with boron trifluoride ($^{10}\text{BF}_3$). The proportional counters are surrounded by 5 cm thick lead and 2 cm thick polyethylene covers. The cross-section of the lead above each section has a surface area of 6 m², and the total surface area of the three sections is 18 m². In the inset to Fig. 6, we show one section of ArNM. The high-energy hadrons and gamma rays from EASs produce multiple neutrons in the lead. Then, the neutrons thermalize in the polyethylene and enter the sensitive volume of the proportional counter to yield Li⁷ and α particles via interactions with boron trifluoride. The α particle accelerates in the high electrical field inside the proportional counter and produces a pulse registered by the DAQ electronics. Suppose only the incident hadrons must be measured (a one-to-one relationship between count rate and hadron flux). In that case, the dead time must equal the secondary neutron collection time ($\approx 1250 \mu\text{s}$) to avoid double-counting. If all pulses need to be counted, the dead time of the NM should be maintained very small. Yuri Stenkin, with colleagues for the first time, described the detection of neutron bursts in the NM related to the occasional hitting of the detector by a core of a high-energy EAS (Stenkin et al., 2007). Hadrons and gamma rays from the EAS core generate numerous thermal neutrons, increasing the NM count rate (neutron multiplicity). This option of EAS core detection by NM was almost not recognized in the past because the usually used long dead time does not permit counting the neutron multiplicity. By establishing a 3000 times shorter dead time of 0.4 μs , we detect EASs hitting ArNM, several of which provide bursts with a neutron multiplicity exceeding 6500, see Fig. 7. The primary particle energies corresponding to this event should be very high ($>10 \text{ PeV}$).

Bursts in the digitizing oscilloscope are observed as sequences of microsecond pulses with spacing equal to at least 100 microseconds. Exhausting information on EAS core hitting ArNM can be found in the dataset of 50 high-multiplicity events published in the Mendeley repository (Soghomonyan et al., 2021). From 50 selected bursts registered by ArNM, we obtain the mean neutron burst durations of $2.6 \pm 0.6 \text{ ms}$. It is approximately 100,000 times larger than the time needed for EAS core particles

to cross the detector. Thus, neutron monitors extend the lifetime of EAS 100,000 times to ms time scales.

6. Discussion and conclusions

Several high-altitude experiments, such as HAWC, LHAASO, and ARGO-YBJ, are searching for Pevatrons, sources of gamma rays with energies up to 10^{15} eV . While a few dozen Pevatron candidates have been identified, the number of PeV particles detected for most sources is limited to 1–2. Therefore, accurately estimating the energy of these particles is crucial. The issue is that enhancing the number of electrons in an atmospheric electric field can lead to energy overestimation, resulting in biases in the declaration of a Pevatron. In a simulation study (Chilingarian, 2023), the results of which are shown in Table 1, the energy of a primary gamma-ray used in the simulation is compared with the calculated, using the “measured” number of electrons (shower size) after EAS crosses the atmospheric electric field. As can be seen from the Table, the calculated energy of the primary gamma rays differs significantly from the “true” values (Lyu et al., 2023). Thus, for the low primary energies (1–10 TeV), the estimated primary gamma-ray energy can be tens-fold higher, for 100 TeV – 6.5 times, and for the higher energies (1 PeV) ≈ 2.5 times.

All experiments (HAWC, LHAASO, ARGO-YBJ, TA, AUGER) report significant changes in the EAS trigger rate and CR intensity coinciding with the movement of the thundercloud. Atmospheric electric fields have less influence on experiments located on sea level (TA, AUGER) compared with high-mountain experiments. The atmospheric electric fields above surface arrays located at sea level are possibly too high, and RREA particles are attenuated before reaching the ground. Therefore, the modulation effects are smaller than at mountain altitudes where the electric field can extend 50–150 m above the ground. The SEVAN detectors located at sea level in Hamburg and Berlin also do not register TGEs. The exception is the winter gamma glow observed on the eastern coast of Japan (Tsuchiya et al., 2007; Wada et al., 2021) because the clouds and electric fields are low due to the specific climatic conditions.

TA and Pierre Auger experiments reported large-scale ($\approx 200 \text{ km}^2$) microsecond duration particle bursts with a source 1–2 km above the Earth’s surface, so-called downward TGFs (DTGFs, Abbasi et al., 2018; Colalillo et al.,

Table 1
“True” and estimated energies of primary gamma rays after passing through the electric field of 2.1 kV/cm strength and 2 km extension.

E_0 (GeV)	Est (GeV)
10^3	2.23×10^4
10^4	1.34×10^5
10^5	6.50×10^5
10^6	2.42×10^6

2023). Unfortunately, only a handful of DTGFs have been detected on the ground, compared with many thousands of TGFs in space. TGFs are brief because of the experimental arrangement located the detector is 400–600 km away from the particle source on the fast-moving satellite. Few from millions of RREA particles born at altitudes ≈ 10 km can reach orbiting detectors; sensors on balloons or aircraft flying just above the equatorial storm will register as many particles as TGEs do (Ostgaard et al., 2023).

In simulations of a standard upward TGF, a point source produces about 10^{17} gamma rays of energy greater than 1 MeV. A similar beam is used to simulate DTGFs. Assuming a point source of gamma rays, located 1–2 km above the ground, creates a footprint of 200 km², a much brighter source is necessary. Placing a radiation source with a fluence greater than 10^{20} gamma rays 1–2 km above the ground is not equivalent to placing it open to space. The energy reaching the Earth would be very high, possibly surpassing that of the Oh-My-God particle observed by the Fly's Eye detector in 1991 (Bird et al., 1995), which had an energy of approximately 50 J.

The distributed radiation model from numerous RREAs originating in a large-scale electric field above particle arrays seems preferable in explaining TGFs and DTGFs. In this model, TGEs and TGFs develop within large-scale strong atmospheric electric fields and do not emerge from an enormously bright point source. The large footprint area of DTGFs can be explained by the large sizes of the atmospheric electric field above the detectors. The atmospheric electric field, lowering to the Earth's surface, can unleash large TGEs that can be detected by horizontally distributed detectors spanning tens of kilometers (Torii et al., 2011; Hisadomi et al., 2021; Chilingarian et al., 2022b). Thus, the driving force of particle bursts is the extended atmospheric electric field and not the atmospheric discharges of any type, creating plenty of seed electrons at a point.

Monitoring particle fluxes, atmospheric discharge, and near-surface electric fields on Aragats provides convincing evidence that TGEs are precursors to lightning flashes. The same conclusion was made by comparing the arrival times of TGFs and spherics (Lindanger et al., 2022). Lightning flashes stop the particle fluxes. They do not initiate them. Lightning initiation involves RREA electrons, which ionize the air and create a channel for the lightning leader to follow (Chilingarian et al., 2017a). The “lightning origin” of the particle bursts confuses the reader with too many uncertainties and contradictions (Luy et al., 2023, and references therein). Invoking poorly understood lightning origin of the particle bursts violates the sufficient reason principle (principium rationis sufficientis cognoscendi). Each meaningful proposition can be considered reliable only if it is sufficiently grounded with arguments that can be regarded as valid. The “lightning” origin of particle bursts also contradicts Occam's razor principle (Entia non sunt multiplicanda praeter necessitate), introducing too many complicated entities (different types of atmospheric

discharges) instead of explaining the particle burst phenomena with more straightforward and well-known phenomena of RREA and EAS. The synergy between cosmic ray physics and atmospheric high-energy physics is instrumental in explaining the particle burst phenomena without invoking complicated and unproven models of atmospheric discharges as the origin of particle bursts.

Declaration of competing interest

The authors declare that they have no known competing financial interests or personal relationships that could have appeared to influence the work reported in this paper.

Acknowledgments

The author thanks the Aragats Space Environmental Center staff for ensuring the seamless operation of experimental facilities on Mount Aragats.

The data underpinning this study can be accessed through the multivariate visualization software platform ADEI, hosted on the CRD webpage of the Yerevan Physics Institute (YerPhI). Interested readers are encouraged to explore the dataset at (ADEI, 2024).

This research effort has been made possible through the support of the Higher Education and Science Committee through Research Project No. 21AG-1C012. The author thanks colleagues from YerPhI for their insightful discussions on TGE-TGF-Lightning problems.

References

- Abbasi, R., Abu-Zayyad, T., Allen, M., et al., 2018. Gamma-ray showers observed at ground level coincidentally with downward lightning leaders. *J. Geophys. Res. Atmos.* 123 (13), 6864–6879. <https://doi.org/10.1029/2017JD027931>.
- Abbasi, R., Abu-Zayyad, T., Allen, M., et al., 2022. Observation of variations in cosmic ray single count rates during thunderstorms and implications for large-scale electric field changes. *Phys. Rev. D* 105. 062002. <https://doi.org/10.1103/PhysRevD.105.062002>.
- Abeysekara, A.U., Aguilar, J.A., Aguilar, S., et al., 2012. On the sensitivity of the HAWC observatory to gamma-ray bursts. *Astropart. Phys.* 35, 641. <https://doi.org/10.1016/j.astropartphys.2012.02.001>.
- ADEI, available online: <http://adei.crd.yerphi.am/> (accessed on 1 January 2024).
- Aglietta, M., Badino, G., Bergamasco, L., et al., 1989. The EAS-TOP array at E0 $1/4 \cdot 10^{14}$ – 10^{16} eV: stability and resolutions. *Nucl. Instrum. Methods Phys. Res. Sect. A* 277, 23–28. [https://doi.org/10.1016/0168-9002\(89\)90531-7](https://doi.org/10.1016/0168-9002(89)90531-7).
- Aharonian, F., An, Q., Axikegu, et al., 2023. Flux variations of cosmic ray air showers detected by LHAASO-KM2A during a thunderstorm on 10 June 2021. *Chin. Phys. C* 47. 015001. <https://doi.org/10.1088/1674-1137/ac3f5b>.
- Alexeenko, V.V., Khaerdinov, N.S., Lidvansky, A.S., et al., 2002. Transient variations of secondary cosmic rays due to atmospheric electric field and evidence for pre-lightning particle acceleration. *Phys. Lett. A* 301, 299–306. [https://doi.org/10.1016/S0375-9601\(02\)00981-7](https://doi.org/10.1016/S0375-9601(02)00981-7).
- Auger, P., Ehrenfest, P., Maze, R., et al., 1939. Extensive cosmic-ray showers. *Rev. Mod. Phys.* 11 (3–4), 288–291. <https://doi.org/10.1103/RevModPhys.11.288>.
- Axikegu, B.B., Bernardini, P., et al., 2022. Cosmic ray shower rate variations detected by the ARGO-YBJ experiment during thunder-

- storms. *Phys. Rev. D* 106. 022008. <https://doi.org/10.1103/PhysRevD.106.022008>.
- Babich, L.P., Donskoy, E.N., Kutsyk, I.M., et al., 2001. Comparison of relativistic runaway electron avalanche rates obtained from Monte Carlo simulations and from kinetic equation solution. *IEEE Trans. Plasma Sci.* 29 (3), 430. <https://doi.org/10.1109/27.928940>.
- Babich, L.P., Donskoy, E.N., Il'kaev, R.I., Kutsyk, I.M., Roussel-Dupre', R.A., 2004. Fundamental parameters of a relativistic runaway electron avalanche in air. *Plasma Phys. Rep.* 30, 616–624. <https://doi.org/10.1134/1.1778437>.
- Bartoli, B., Bernardini, P., Bi, X.J., 2016. Detection of thermal neutrons with the PRISMA- YBJ array in extensive air showers selected by the ARGO-YBJ experiment. *Astropart. Phys.* 81, 49–60. <https://doi.org/10.1016/j.astropartphys.2016.04.007>.
- Bird, D.J., Corbato, S.C., Dai, H.Y., et al., 1995. Detection of a cosmic ray with measured energy well beyond the expected spectral cutoff due to cosmic microwave radiation. *Astrophys. J.* 441, 144. <https://doi.org/10.1086/175344>.
- BOLTEK, available online: https://www.boltek.com/EFM-100C_Manual_030323.pdf (accessed on 1 January 2024).
- Bowers, G.S., Shao, X.-M., Blaine, W., et al., 2021. Fairweather neutron bursts from photonuclear reactions by extensive air shower core interactions in the ground and implications for terrestrial gamma-ray flash signatures. *Geophys. Res. Lett.* 48. e2020GL090033. <https://doi.org/10.1029/2020GL090033>.
- Briggs, M.S., Xiong, S., Connaughton, V., Tierney, D., Fitzpatrick, G., Foley, S., et al., 2013. Terrestrial gamma-ray flashes in the Fermi era: improved observations and analysis methods. *J. Geophys. Res.: Space Phys.* 118 (6), 3805–3830. <https://doi.org/10.1002/jgra.50205>.
- Celestin, S., Pasko, V.P., 2011. Energy and fluxes of thermal runaway electrons produced by exponential growth of streamers during the stepping of lightning leaders and in transient luminous events. *J. Geophys. Res. (space Phys.)* 116, 3315. <https://doi.org/10.1029/2010JA016260>.
- Chilingarian, A., 2023. Thunderstorm Ground Enhancements measured on Aragats and progress of high-energy physics in the atmosphere. *Atmosphere* 14, 300. <https://doi.org/10.3390/atmos14020300>.
- Chilingarian, A., Gharagozyan, H.G., et al., 2004. Light and heavy cosmic-ray mass group energy spectra as measured by the MAKET-ANI detector. *Astrophys. J.* 603, L29. <https://doi.org/10.1086/383086>.
- Chilingarian, A., Hovsepian, G., 2021. Dataset for 16 parameters of ten thunderstorm ground enhancements (TGEs) allowing recovery of electron energy spectra and estimation the structure of the electric field above Earth's surface. *Mendeley Data V3*. <https://doi.org/10.17632/tvbn6wdf85.3>.
- Chilingarian, A., Chilingaryan, S., Karapetyan, T., Kozliner, L., Khanikyants, Y., Hovsepian, G., Pokhsroryan, D., Soghomonyan, S., 2017a. On the initiation of lightning in thunderclouds. *Scientific Reports* 7. 1371. <https://doi.org/10.1038/s41598-017-01288-0>.
- Chilingarian, A., Hovsepian, G., Elbekian, A., Karapetyan, T., Kozliner, L., Martoian, H., Sargsyan, B., 2019b. Origin of enhanced gamma radiation in thunderclouds. *Phys. Rev. Res.* 1. 033167. <https://doi.org/10.1103/PhysRevResearch.1.033167>.
- Chilingarian, A., Hovsepian, G., Sargsyan, B., 2020a. Circulation of radon progeny in the terrestrial atmosphere during thunderstorms. *Geophys. Res. Lett.* 47. e2020GL091155. <https://doi.org/10.1029/2020GL091155>.
- Chilingarian, A., Hovsepian, G., Svechnikova, E., Zazyan, M., 2021a. Electrical structure of the thundercloud and operation of the electron accelerator inside it. *Astropart. Phys.* 132. 102615. <https://doi.org/10.1016/j.astropartphys.2021.102615>.
- Chilingarian, A., Hovsepian, G., Zazyan, M., 2021b. Measurement of TGE particle energy spectra: an insight in the cloud charge structure. *Europhys. Lett.* 134, 6901. <https://doi.org/10.1209/0295-5075/ac0dfa>.
- Chilingarian, A., Hovsepian, G., 2022. The synergy of the cosmic ray and high energy atmospheric physics: Particle bursts observed by arrays of particle detectors. *New Astron.* 97. 101871. <https://doi.org/10.1016/j.newast.2022.101871>.
- Chilingarian, A., Hovsepian, G., Kazaryan, S., et al., 2005. Correlated measurements of secondary cosmic ray fluxes by the aragats space-environmental center monitors. *Nucl. Instrum. Methods A* 543, 483. <https://doi.org/10.1016/j.nima.2004.12.021>.
- Chilingarian, A., Hovsepian, G., Arakelyan, K., Chilingaryan, S., Danielyan, V., Avakyan, K., et al., 2009. Space environmental viewing and analysis network (SEVAN). *Earth Moon Planets* 104, 195. <https://doi.org/10.1007/s11038-008-9288-1>.
- Chilingarian, A., Daryan, A., Arakelyan, K., et al., 2010. Ground-based observations of thunderstorm-correlated fluxes of high-energy electrons, gamma rays, and neutrons. *Phys. Rev. D* 82. 043009. <https://doi.org/10.1103/PhysRevD.82.043009>.
- Chilingarian, A., Hovsepian, G., Hovhannisyian, A., 2011. Particle bursts from thunderclouds: natural particle accelerators above our heads. *Phys. Rev. D* 83. 062001. <https://doi.org/10.1103/PhysRevD.83.062001>.
- Chilingarian, A., Hovsepian, G., Khanikyanc, Y., Reymers, A., Soghomonyan, S., 2015. Lightning origination and thunderstorm ground enhancements terminated by the lightning flash. *Europhys. Lett.* 110. 49001. <https://doi.org/10.1209/0295-5075/110/49001>.
- Chilingarian, A., Khanikyants, Y., Mareev, E., Pokhsroryan, D., Rakov, V.A., Soghomonyan, S., 2017b. Types of lightning discharges that abruptly terminate enhanced fluxes of energetic radiation and particles observed at ground level. *J. Geophys. Res. Atmos.* 122, 7582–7599. <https://doi.org/10.1002/2017JD026744>.
- Chilingarian, A., Mkrtchyan, H., Karapetyan, T., Chilingaryan, S., Sargsyan, B., Arestakesyan, A., 2019a. Catalog of 2017 Thunderstorm Ground Enhancement (TGE) events observed on Aragats. *Nat. Sci. Rep.* 9 (1), 6253. <https://doi.org/10.1038/s41598-019-42786-7>.
- Chilingarian, A., Khanikyants, Y., Rakov, V.A., Soghomonyan, S., 2020b. Termination of thunderstorm-related bursts of energetic radiation and particles by inverted intracloud and hybrid lightning discharges. *Atmos. Res.* 233. 104713. <https://doi.org/10.1016/j.atmosres.2019.104713>.
- Chilingarian, A., Karapetyan, T., Zazyan, M., Hovsepian, G., Sargsyan, B., Nikolova, N., Angelov, H., Chum, J., Langer, R., 2021d. Maximum strength of the atmospheric electric field. *Phys. Rev. D* 103. 043021. <https://doi.org/10.1103/PhysRevD.103.043021>.
- Chilingarian, A., Kozliner, L., Sargsyan, B., Soghomonyan, S., Chilingaryan, S., Pokhsroryan, D., Zazyan, M., 2022a. Thunderstorm ground enhancements: multivariate analysis of 12 years of observations. *Phys. Rev. D* 106. 082004. <https://doi.org/10.1103/PhysRevD.106.082004>.
- Chilingarian, A., Hovsepian, G., Karapetyan, T., Kozliner, L., Chilingaryan, S., Pokhsroryan, D., Sargsyan, B., 2022b. The horizontal profile of the atmospheric electric fields as measured during thunderstorms by the network of NaI spectrometers located on the slopes of Mt. Aragats. *J. Instrum.* 17, P10011. <https://doi.org/10.1088/1748-0221/17/10/P10011>.
- Chilingarian, A., Hovsepian, G., Karapetyan, T., et al., 2022c. Multimessenger observations of thunderstorm-related bursts of cosmic rays. *J. Instrum.* 17, P07022. <https://doi.org/10.1088/1748-0221/17/07/P07022>.
- Chilingarian, A., Hovsepian, G., Karapetyan, T., Sargsyan, B., Chilingaryan, S., 2022d. Measurements of energy spectra of relativistic electrons and gamma-rays avalanches developed in the thunderous atmosphere with Aragats Solar Neutron Telescope. *J. Instrum.* 17, P03002. <https://doi.org/10.1088/1748-0221/17/03/P03002>.
- Chilingarian, A., Hovsepian, G., Aslanyan, D., Sargsyan, B., Karapetyan, T., 2022f. Catalog of Thunderstorm Ground Enhancements (TGEs) observed at Aragats in 2013–2021. *Mendeley Data VI*. <https://doi.org/10.17632/8gtdbch59z.1>.
- Chilingarian, A., Hovsepian, G., Aslanyan, D., Karapetyan, T., Sargsyan, B., Zazyan, M., 2023a. TGE electron energy spectra: comment on “Radial diagnosis of the thundercloud electron accelerator” by E. Williams et al. (2022). *J. Geophys. Res.: Atmos.* 128. <https://doi.org/10.1029/2022JD037309>.

- Chilingarian, A., Hovsepyan, G., Karapetyan, T., Aslanyan, D., Chilingaryan, S., Sargsyan, B., 2023b. Genesis of thunderstorm ground enhancements. *Phys. Rev. D* 107, 102003. <https://doi.org/10.1103/PhysRevD.107.102003>.
- Chilingarian, A., Pokhsranyan, D., Zagumenov, F., Zazyan, M., 2024a. Space-temporal structure of the thunderstorm ground enhancements (TGEs). *Phys. Open* 18, 100202. <https://doi.org/10.1016/j.physo.2023.100202>.
- Chilingarian, A., Karapetyan, T., Sargsyan, B., Knapp, J., Walter, M., Rehm, T., 2024b. Energy spectra of the first TGE observed on Zugspitze by the SEVAN light detector compared with the energetic TGE observed on Aragats. *Astropart. Phys.* 156, 02924. <https://doi.org/10.1016/j.astropartphys.2024.102924>.
- Chilingarian, A., Karapetyan, T., Aslanyan, D., Sargsyan, B., 2024c. Extreme thunderstorm ground enhancements registered on Aragats in 2023. *Mendeley Data V1*. <https://doi.org/10.17632/z4ry54hccb.1> <https://data.mendeley.com/datasets/z4ry54hccb/1>.
- Chubenko, A.P., Shepetov, A.L., Antonova, V.P., et al., 2016. New complex EAS installation of the Tien Shan mountain cosmic ray station. *Nucl. Instrum. Methods A* 832, 158. <https://doi.org/10.1016/j.nima.2016.06.068>.
- Chum, R., Langer, J., Baše, M., Kollárik, I., Strhářský, G., Diendorfer, J. R., 2020. Significant enhancements of secondary cosmic rays and electric field at high mountain peak during thunderstorms. *Earth Planets Space* 72, 28. <https://doi.org/10.1186/s40623-020-01155-9>.
- Colalillo, R., for the Pierre Auger Collaboration, 2023. The Pierre Auger Observatory: studying atmospheric electricity with cosmic-ray detectors. *Eur. Phys. J. Web Conf.* 283, 06014. <https://doi.org/10.1051/epjconf/202328306014>.
- Dwyer, J.R., 2003. A fundamental limit on electric fields in air. *Geophys. Res. Lett.* 30, 2055. <https://doi.org/10.1029/2003GL017781>.
- Dwyer, J.R., 2007. Relativistic breakdown in planetary atmospheres. *Phys. Plasmas* 14, 042901. <https://doi.org/10.1063/1.2709652>.
- Dwyer, J.R., Smith, D.M., Cummer, S.A., 2012. High-energy atmospheric physics: terrestrial gamma-ray flashes and related phenomena. *Space Sci. Rev.* 173, 133. <https://doi.org/10.1007/s11214-012-9894-0>.
- Fishman, G.J., Bhat, P.N., Mallozzi, R., et al., 1994. Discovery of intense gamma-ray flashes of atmospheric origin. *Science* 264, 1313. <https://doi.org/10.1126/science.264.5163.1313>.
- Fuglestad, A.N., 2023. Multi Pulse Gamma-ray Flashes and optical pulses of lightning observed by ASIM, Master Thesis. In: *Space Physics*. University of Bergen. <https://bora.uib.no/bora-xmlui/bitstream/handle/11250/3073302/Multi-Pulse-TYerrestrial-Gamma-ray-Flashes-and-optical-pulses-of-lightning-observed-by-ASIM-print-version.pdf?sequence=3&isAllowed=y>.
- Gurevich, A.V., Milikh, G.M., Roussel-Dupre, R.A., 1992. Runaway electron mechanism of air breakdown and preconditioning during a thunderstorm. *Phys. Lett.* 165A, 463. [https://doi.org/10.1016/0375-9601\(92\)90348-P](https://doi.org/10.1016/0375-9601(92)90348-P).
- Gurevich, A.V., Zybin, K.P., Roussel-Dupre, R.A., 1999. Lightning initiation by simultaneous runaway breakdown and cosmic ray showers. *Phys. Lett. A* 254, 79. [https://doi.org/10.1016/S0375-9601\(99\)00091-2](https://doi.org/10.1016/S0375-9601(99)00091-2).
- Heck, D., Knapp, J., Capdevielle, J.N., Schatz, G., Thouw, T., 1998. Forschungszentrum (Nuclear Research Center), Karlsruhe, Report No. FZKA 6019. <https://www.ikp.kit.edu/corsika/70.php>.
- Hisadomi, S., Nakazawa, K., Wada, Y., et al., 2021. Multiple gamma-ray glows, and a dawnward TGF observed from nearby thunderclouds. *J. Geophys. Res. Atmos.* 126, e2021JD034543. <https://doi.org/10.1029/2021jd034543>.
- Izhbulyakova, Z.T., Bogdanov, A.G., Bogdanov, F.A., et al., 2020. Investigation of the EAS neutron component with the URAN array: first simulation and experimental results. *J. Phys. Conf. Ser.* 1690, 012071. <https://doi.org/10.1088/1742-6596/1690/1/012071>.
- Kelley, N.A., Smith, D.M., Dwyer, J.R., et al., 2015. Relativistic electron avalanches as a thunderstorm discharge competing with lightning. *Nat. Commun.* 6 (7845). <https://doi.org/10.1038/ncomms8845>.
- Kochkin, P., Van Deursen, P., Marisaldi, M., et al., 2017. In-flight observation of gamma-ray glows by ILDAS. *JGR Atmos.* 122, 12801–12811. <https://doi.org/10.1002/2017JD027405>.
- Kuettner, J., 1950. The electrical and meteorological conditions inside thunderclouds. *J. Meteorol.* 7, 322–332. [https://doi.org/10.1175/1520-0469\(1950\)007<0322:TEAMCI>2.0.CO;2](https://doi.org/10.1175/1520-0469(1950)007<0322:TEAMCI>2.0.CO;2).
- Lara, A., De Raga, G.B., Enriques-Rivera, O., 2017. HAWC response to atmospheric electricity activity. In: *Proceedings of 35th International Cosmic Ray Conference, 2017, Bexco, Busan, Korea*, <https://doi.org/10.48550/arXiv.1711.04202>.
- Li, B.-B., Alekseenko, V.V., Cui, S.-W., et al., 2017. EAS thermal neutron detection with the PRISMA-LHAASO-16 experiment. *J. Instrum.* 12, P12028. <https://doi.org/10.1088/1748-0221/12/12/P12028>.
- Lindanger, A., Skeie, C.A., Marisaldi, M., Bjørge-Engeland, I., Østgaard, N., Mezentsev, A., et al., 2022. Production of terrestrial gamma-ray flashes during the early stages of lightning flashes. *J. Geophys. Res.: Atmos.* 127, e2021JD036305. <https://doi.org/10.1029/2021JD036305>.
- Lyu, F., Zhang, Y., Lu, G., Zhu, B., Zhang, H., Xu, W., Xiong, S., Liu, W., 2023. Recent observations and research progress of terrestrial gamma-ray flashes during thunderstorms. *Sci. China Earth Sci.* 66. <https://doi.org/10.1007/s11430-022-1026-y>.
- Mailyan, B.G., Briggs, M.S., Cramer, E.S., et al., 2016. The spectroscopy of individual terrestrial gamma-ray flashes: constraining the source properties. *J. Geophys. Res. Space Phys.* 121, 11346–11363. <https://doi.org/10.1002/2016JA022702>.
- Marisaldi, M., Fuschino, F., Labanti, C., Galli, M., Longo, F., Del Monte, E., et al., 2010. Detection of terrestrial gamma-ray flashes up to 40 MeV by the AGILE satellite. *J. Geophys. Res.* 115 (A3). <https://doi.org/10.1029/2009JA014502>.
- Marshall, T.C., McCarthy, M.P., Rust, W.D., 1995. Electric field magnitudes and lightning initiation in thunderstorms. *J. Geophys. Res.* 100, 7097. <https://doi.org/10.1029/95JD00020>.
- McCarthy, M., Parks, G., 1985. Further observations of X-rays inside thunderstorms. *Geophys. Res. Lett.* 12, 393. <https://doi.org/10.1029/GL012i006p00393>.
- Moraal, H., Belov, A., Clem, J.M., 2000. Design and co-ordination of Multistation International Neutron Monitor Networks. *Space Sci. Rev.* 93, 285. <https://doi.org/10.1023/A:1026504814360>.
- Nag, A., Rakov, V., 2009. Some inferences on the role of lower positive charge region in facilitating different types of lightning. *Geophys. Res. Lett.* 36, L05815. <https://doi.org/10.1029/2008GL036783>.
- Neubert, T., Østgaard, N., Reglero, V., Blanc, E., Chanrion, O., Oxborrow, C.A., et al., 2019. The ASIM mission on the International Space Station. *Space Sci. Rev.* 215 (2), 26. <https://doi.org/10.1007/s11214-019-0592-z>.
- Ostgaard, N., Christian, H.J., Grove, J.E., Sarria, D., Mezentsev, A., Kochkin, P., et al., 2019. Gamma-ray glow observations at 20-km altitude. *J. Geophys. Res. Atmos.* 124, 7236–7254. <https://doi.org/10.1029/2019JD030312>.
- Ostgaard, N., Lang, T.G., Marisaldi, M., et al., 2023. Results from the ALOFT mission: a flight campaign for TGF and gamma-ray glow observations over Central America and the Caribbean in July 2023, AGU, San Francisco 2023, AE22A-03. <https://doi.org/10.5194/egu-sphere-egu23-3116>.
- Pallu, M., Celestin, S., Hazem, Y., Trompier, F., Patton, G., 2023. XStorm: a new gamma-ray spectrometer for detecting proximity gamma-ray glows and TGFs. *J. Geophys. Res.: Atmos.* 128, e2023JD039180. <https://doi.org/10.1029/2023JD039180>.
- Parks, G.K., Mauk, B.H., Spiger, R., Chin, J., 1981. X-ray enhancements detected during thunderstorm and lightning activities. *Geophys. Res. Lett.* 8, 1176–1179. <https://doi.org/10.1029/GL08i011p01176>.
- Pokhsranyan, D., 2016. Fast Data Acquisition system based on NI-myRIO board with GPS time stamping capabilities for atmospheric electricity research. In: *Proceedings of TEPA symposium, Nor Amberd, 2015, p.23, "Tigran Mets," Yerevan*. <https://inspirehep.net/conferences/1407534>.
- Roussel-Dupré, R., Symbalisty, E., Taranenko, Y., Yukhimuk, V., 1998. Simulations of high-altitude discharges initiated by runaway break-

- down. *J. Atmos. Sol.-Terr. Phys.* 60, 917–940. [https://doi.org/10.1016/S1364-6826\(98\)00028-5](https://doi.org/10.1016/S1364-6826(98)00028-5).
- Skeie, C.A., Østgaard, N., Mezentsev, A., Bjørge-Engeland, I., Marisaldi, M., Lehtinen, N., et al., 2022. The temporal relationship between terrestrial gamma-ray flashes and associated optical pulses from lightning. *J. Geophys. Res.: Atmos.* 127. e2022JD037128. <https://doi.org/10.1029/2022JD037128>.
- Smith, D.M., Lopez, L.I., Lin, R.P., Barrington-Leigh, C., 2005. Terrestrial gamma-ray flashes observed up to 20 MeV. *Science* (new York, n.y.) 307, 1085–1088. <https://doi.org/10.1126/science.1107466>.
- Soghomonyan, S., Chilingarian, A., Khanikyants, Y., 2021a. Dataset for thunderstorm ground enhancements terminated by lightning discharges. *Mendeley Data V1*.
- Soghomonyan, S., Chilingarian, A., Pokhsranyan, D., 2021b. Extensive air shower (EAS) registration by the measurements of the multiplicity of neutron monitor signal". *Mendeley Data V1*. <https://doi.org/10.17632/43ndcktj3z.1>.
- Stenkin, Y., Djappuev, D.D., Valdés-Galicia, J.F., 2007. Neutrons in extensive air showers. *Phys. at. Nucl.* 70, 1088. <https://doi.org/10.1134/S1063778807060117>.
- Stenkin, Y., 2009. Nuclear Track Detectors: Design, Methods and Applications. In: Sidorov, M., Ivanov, O., (Eds.) Nova Science Publishers, Inc. Chapter 10, ISBN: 978-1-60876-826-4.
- Stolzenburg, M., Marshall, T.C., Rust, W.D., Bruning, E., MacGorman, D.R., Hamlin, T., 2007. Electric field values observed near lightning flash initiations. *Geophys. Res. Lett.* 34, L04804. <https://doi.org/10.1029/2006GL028777>.
- Torii, T., Sugita, T., Kamogawa, M., et al., 2011. Migrating source of energetic radiation generated by thunderstorm activity. *Geophys. Res. Lett.* 38, L24801. <https://doi.org/10.1029/2011GL049731>.
- Trinh, T.N.G., Scholten, O., Buitink, S., Ebert, U., Hare, B.M., Krehbiel, P.R., et al., 2020. Determining electric fields in thunderclouds with the radiotelescope LOFAR. *J. Geophys. Res.: Atmos.* 125. e2019JD031433. <https://doi.org/10.1029/2019JD031433>.
- Tsuchiya, H., Enoto, T., Yamada, S., et al., 2007. Detection of high-energy gamma rays from winter thunderclouds. *Phys. Rev. Lett.* 99. 165002. <https://doi.org/10.1103/PhysRevLett.99.165002>.
- Wada, Y., Matsumoto, T., Enoto, T., et al., 2021. Catalog of gamma-ray glow during four winter seasons in Japan. *Phys. Rev. Res.* 3. 043117. <https://doi.org/10.1103/PhysRevResearch.3.043117>.
- Zhang, H., Lu, G., Liu, F., Xiong, S., Ahmad, M.R., Yi, Q., et al., 2021. On the terrestrial gamma-ray flashes preceding narrow bipolar events. *Geophys. Res. Lett.* 48. e2020GL092160. <https://doi.org/10.1029/2020GL092160>.